academicJournals

Vol. 8(43), pp. 2011-2022, 23 November, 2013
DOI: 10.5897/IJPS2013.4051
ISSN 1992 - 1950 © 2013 Academic Journals
http://www.academicjournals.org/IJPS

International Journal of Physical Sciences

Full Length Research Paper

Optimization of the louver angle and louver pitch for a louver finned and tube heat exchanger

Jiin-Yuh Jang* and Chun-Chung Chen

Department of Mechanical Engineering, National Cheng Kung University, Tainan 70101, Taiwan.

Accepted 14 November, 2013

The optimization of the louver angle (θ) and the louver pitch (Lp) for a louver finned and tube heat exchanger was investigated numerically along with a simplified conjugate-gradient method (SCGM). The area reduction ratio relative to a plain surface is the objective function to be maximized. A search for the optimum louver angle (θ) and louver pitch (Lp), ranging from 15°< θ < 40° and 2 mm < Lp < 3.2 mm, respectively, was performed. The results showed that the maximum area reduction ratios may reach 39~46% combined with the optimal design of (θ, Lp) at Re_D = 589~3533 (U_{in}= 0.5-3.0 m/s).

Key words: Optimization, louver pitch, louver angle, finned and tube heat exchanger.

INTRODUCTION

Fin-and-tube heat exchangers with louvered fins are widely employed in automobiles, air-conditioners and power generation, etc. The louvers act to interrupt the airflow and create a series of thin boundary layers that have lower thermal resistance. The first reliable published data on louvered fin surfaces was presented by Kays and London (1950). Davenport (1983) utilized smoke trace to study a standard variant of the corrugated louvered fin geometry and obtained heat transfer and friction correlations for corrugated louvered fin geometry. Achaichia and Cowell (1988) made an overall study of performance characteristics of flat-sided tube and louvered plate fin heat exchangers. They obtained the correlations for the louvered plate fin geometry. Sahnoun and Webb (1992) developed an analytical model to predict the heat transfer and friction characteristics of the corrugated louvered fin core. Sunden and Svantesson (1992) presented the investigations of heat transfer and pressure drop of standard louver fin and inclined louver fin. Their investigations illustrate that all the louvered surfaces are better efficient than the corresponding smooth surface. Wang et al. (1998) tested 17 samples of commercially available louver fin and tube heat exchangers for different geometrical parameters, including the number of tube row, fin pitch, and tube size.

In the 1990's, some investigators developed CFD code based on non-orthogonal, boundary-fitted meshes to calculate the flow over louvered fins. Suga et al. (1990) and Suga and Aoki (1991) used a rectangular flow domain filled with overlapping Cartesian meshes to calculate the flow and heat transfer over a finite-thickness fin. Hiramatsu et al. (1990) and Ikuta et al. (1990) utilized a block structured mesh with respective blocks for each louver.

Jang et al. (2001) numerically researched a three dimensional convex louver finned tube heat exchangers. The effects of different geometrical factor, containing convex louver angles (15.5°, 20.0°, 24.0°), louver pitch (0.953 mm, 1.588 mm) and fin pitch (8 fins/in., 10 fins/in., 15 fins/in.) are studied in detail for the Reynolds number ranging from 100 to 1100. It was proven that, for equal louver pitch, both the average Nusselt number and pressure drop coefficient are increased as the louver angle is increased; while for equal louver angles, they are

*Corresponding author. E-mail: jangjim@mail.ncku.edu.tw, Tel: +886-6-2757575 ext. 62148, Fax: +886-6-2088573.

decreased as the louver pitch is increased. Hsieh and Jang (2006) proposed continuously increased or decreased louver angle models and carried out a 3-D numerical analysis on heat transfer and fluid flow. Their results showed that continuously variable louver angle types employed in heat exchangers could effectively enhance the heat transfer performance. They also revealed that the maximum area reduction could reach up to 25.5% compared with a plain fin surface. Jang and Tsai (2011) utilized the simplified conjugate-gradient method (SCGM) to search the optimal louver angle of a fin heat exchanger. The area reduction for using louver surface compared to the plain surface was the objective function to be maximized. The maximum area reduction ratios of the louvered fins were 65.3, 66.9, 65.6, 63.7 and 62.2% with Re = 100 ~ 500 and Lp = 1.0 mm. Hsieh and Jang (2012) numerically studied the optimal design of a louver finned-tube heat exchanger applying the Taguchi method. Eighteen kinds of patterns were made by mixed levels on each factor. The optimal design values for each parameter were all reported.

The foregoing literature review reveals that no related 3-D numerical analysis for the optimization of louvered angle and louvered pitch and their coupled effects on the thermal and hydraulic characteristics of a louver finned and tube heat exchanger has been published. This has motivated the present investigation. In the present research, the optimization of louver angle and its pitch is studied and solved numerically using a commercial CFD code ANSYS FLUENT (2009) along with a simplified conjugate-gradient method. To achieve optimization goals, the area reduction ratio is the objective function to be maximized. The influence of louver pitch (Lp = 2.0 ~ 3.2 mm) and louver angle (θ = 15°< θ < 40°) on the heat transfer performance and friction loss at different Reynolds numbers are discussed in detail. The optimal design values for two operating parameters at different Reynolds number are also presented.

MATHEMATICAL ANALYSIS

Governing equation

Figure 1 describes the physical model and relevant geometric dimensions of the louver finned and tube heat exchanger. The unit is a mini-meter. The louver angle (θ = 15° ~ 40°) and louver pitch (Lp = 2.0 ~ 3.2 mm) as shown in Figure 2 are the main operating parameters in the present study. The fluid is considered 3-D incompressible turbullent flow with constant properties, and the flow is assumed to be steady with no viscous dissipation. Equations for continuity, momentum (Reynolds averaged Navier-Stokes equations), energy, turbulent kinetic energy, k, and the dissipation rate, ε, can be expressed in tensor form as follows:

$$\frac{\partial \overline{u_i}}{\partial x_i} = 0 \tag{1}$$

$$\frac{\partial}{\partial x_j}\rho\left(\overline{u_i u_j}\right) = -\frac{\partial \overline{P}}{\partial x_i} + \frac{\partial}{\partial x_j}\left[\mu_{eff}\left(\frac{\partial \overline{u_i}}{\partial x_j} + \frac{\partial \overline{u_j}}{\partial x_i}\right) - \rho\left(\overline{u_i' u_j'}\right)\right] \tag{2}$$

$$\frac{\partial}{\partial x_j}\rho C\left(\overline{u_j T}\right) = \overline{u_j}\frac{\partial \overline{P}}{\partial x_j} + \overline{u_j'}\frac{\partial \overline{P'}}{\partial x_j} + \frac{\partial}{\partial x_j}\left[k\frac{\partial \overline{T}}{\partial x_j} - \rho C\overline{u_j' T'}\right] \tag{3}$$

$$\frac{\partial}{\partial x_i}\left(\rho\overline{u_i}k\right) = -\frac{\partial}{\partial x_i}\left(\frac{\mu_{eff}}{\sigma_k}\frac{\partial k}{\partial x_i}\right) + \rho(\mathrm{Pr} - \varepsilon) \tag{4}$$

$$\frac{\partial}{\partial x_i}\left(\rho\overline{u_i}\varepsilon\right) = -\frac{\partial}{\partial x_i}\left(\frac{\mu_{eff}}{\sigma_\varepsilon}\frac{\partial \varepsilon}{\partial x_i}\right) + \rho\frac{\varepsilon}{k}\left[\left(c_1 + c_3\frac{\mathrm{Pr}}{\varepsilon}\right)\mathrm{Pr} - c_2\varepsilon\right] \tag{5}$$

where $\mathrm{Pr} = (\mu_t/\rho)[2(\partial u_i/\partial x_i)^2 - 2(\nabla u_i)^2/3]$, $\mu_{eff} = \mu + \mu_t$, $\mu_t = \rho c_\mu\left(k^2/\varepsilon\right)$, $c_\mu = 0.09$, $c_1 = 0.15$, $c_2 = 1.90$, $c_3 = 0.25$, $\sigma_k = 0.75$ *and* $\sigma_\varepsilon = 1.15$

Equation 2 contains Reynolds stresses that are modeled by Chen's extended k-ε turbulence model (Chen and Kim, 1987; Wang and Chen, 1993), where k is the turbulent kinetic energy, and ε is the dissipation rate. In Chen's model, the production time scale as well as the dissipation time scale is used in closing the ε equation. This extra production time scale is claimed to allow the energy transfer mechanism of turbulence to respond to the mean strain rate more effectively. This results in an extra constant in the ε equation. As to the velocity distribution in the near-wall region ($y^+ \leq 11.63$), the following law of the wall (Liakopoulos, 1984) is applied:

$$u^+ = \ln\left[\frac{(y^+ + 11)^{4.02}}{(y^{+2} - 7.37y^+ + 83.3)^{0.79}}\right] + 5.63\tan^{-1}(0.12y^+ - 0.441) - 3.81 \tag{6}$$

Where

$$y^+ \equiv \frac{\rho u_\tau y}{\mu} \text{ and } u_\tau = \sqrt{\frac{\tau_w}{\rho}} \tag{7}$$

Parameter definition of performance factor

The local pressure drop can be expressed in terms of the dimensionless pressure coefficient C_p defined as:

$$Cp = \frac{p - p_{in}}{\frac{1}{2}\rho U_{in}^2} \tag{8}$$

where P_{in} is the pressure at inlet and U_{in} is the inlet velocity. The local heat transfer coefficient *h* is defined as:

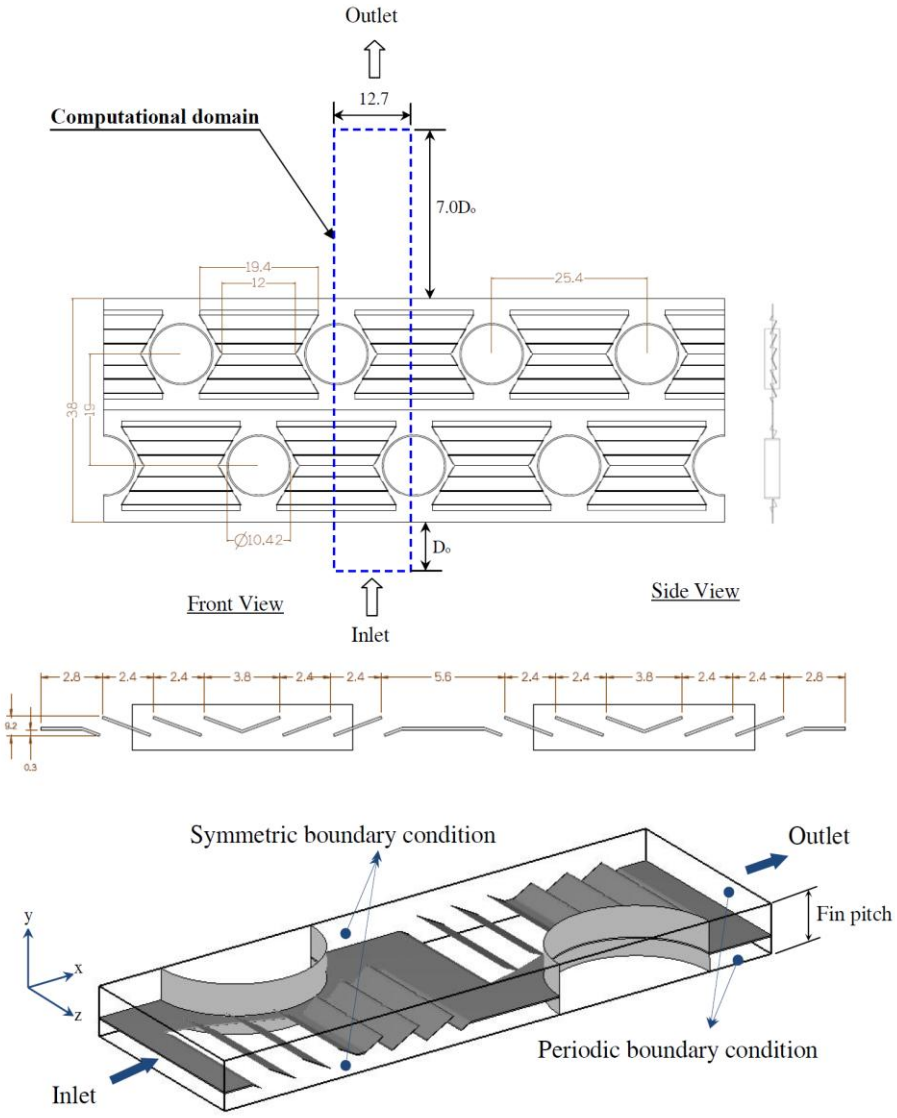

Figure 1. The physical model and computational domain (fin thickness, t =0.115 mm).

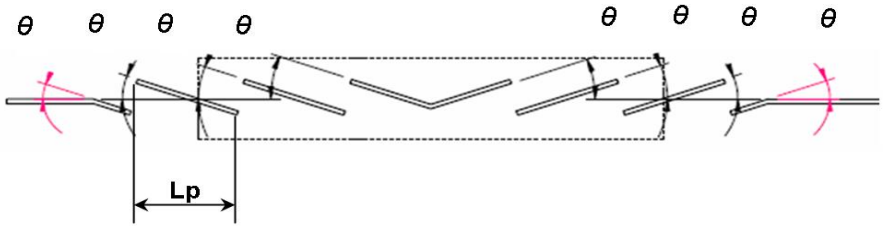

Louver angle θ	15°	20°	25°	30°	35°	40°
Louver pitch Lp	2.0mm	2.2mm	2.4mm	2.6mm	2.8mm	3.0mm	3.2mm

Figure 2. The louver pattern for different louver angles and louver pitches.

$$h = \frac{q''}{T_w - T_b} \tag{9}$$

where q'' is the local heat flux. T_b is the local bulk mean temperature. T_w is the wall temperature. The local heat transfer coefficient can be expressed in the dimensionless form by the Nusselt number *Nu*, defined as:

$$Nu = \frac{h \cdot D_o}{k} = \frac{\partial \left[\frac{\Theta}{\Theta_b} \right]_{wall} \cdot D_o}{\partial \, n} \tag{10}$$

where $\Theta_b = (T_b - T_{in})/(T_w - T_{in})$ is the local dimensionless bulk mean temperature and *n* is the dimensionless unit vector normal to the wall and D_o is the outside diameter of tube. The average Nusselt number $\overline{Nu}$ can be obtained by

$$\overline{\mathrm{Nu}} = \frac{\int \mathrm{Nu} \, \mathrm{dA_s}}{\int \mathrm{dA_s}} \tag{11}$$

where dA_s is the infinitesimal area of the wall surface. The friction factor f and Colburn factor j are defined as:

$$f = \frac{p - p_{in}}{\frac{1}{2} \rho U_{in}^{\ 2}} \times \frac{D_o}{4L} \tag{12}$$

$$j = \frac{\overline{\mathrm{Nu}}}{\mathrm{Re}_D \mathrm{Pr}^{1/3}} \tag{13}$$

where P_{in} is the pressure at the inlet, L is the flow length, Re_D is the Reynolds number defined as $\mathrm{Re}_D = \mathrm{U_{max}} \mathrm{D_o} / \nu$, U_{max} is the air velocity at minimum free flow area, Pr is the Prandtal number defined as $\mathrm{Pr} = \nu / \alpha$, α is the thermal diffusivity, and v is the kinematic viscosity.

Boundary condition

Since the governing equations are elliptic, it is necessary to impose boundary conditions at all of the boundaries in the computational domain. The upstream boundary is established at a distance of one tube diameter in front of the leading edge of the fin. At this boundary, the flow velocity U_{in} is assumed to be uniform, and the temperature T_{in} is taken to be 300K. At the downstream end of the computational domain, located seven times the tube diameter from the last downstream row tube, the streamwise gradients (Neumann boundary conditions) for all the variables are set to zero. At the solid surfaces, no-slip conditions and constant wall temperature T_W (353K) are specified. On the symmetry planes (two X-Y planes), normal gradients are set to zero. On the upper and lower X-Z planes, periodic boundary conditions are imposed. Additionally, at the solid-fluid interface,

$$\mathrm{T_s} = T_f \; ; \; -k_s \cdot \partial T_s / \partial n = -k_f \cdot \partial T_f / \partial n \tag{14}$$

Performance evaluation criteria (PEC)

Many performance evaluation criteria (PEC) have been developed for evaluating the performance of heat exchangers. The VG-1 (variable geometry) performance criteria, as described by Webb (1994), represents the possibility of surface area reduction by using enhanced surfaces having fixed heat duty, temperature difference and pumping power.

$$\frac{hA}{h_o A_o} = \frac{j}{j_o} \frac{A}{A_o} \frac{G}{G_o} \tag{15}$$

where the subscripts of 'o' refer to the reference plate fin, and *G* is the mass velocity. The pumping power is calculated as:

$$\omega = \left(f \frac{A}{A_m} \frac{G^2}{2\rho} \right) \left(\frac{G A_m}{\rho} \right) \tag{16}$$

where A_m is the flow area at minimum cross section. The pumping power ratio relative to the reference plane fin can be obtained by:

$$\frac{\omega}{\omega_o} = \frac{f}{f_o} \frac{A}{A_o} \left(\frac{G}{G_o} \right)^3 \tag{17}$$

and by the elimination of the term

$$\frac{hA / h_o A_o}{(\omega / \omega_o)^{1/3} (A / A_o)^{2/3}} = \frac{j / j_o}{(f / f_o)^{1/3}} \tag{18}$$

Under the pumping power constraint of case VG-1, that is ($\omega/\omega_o = 1$), we may obtain the area reduction ratio relative to the reference plane fin as:

$$\frac{A}{A_o} = \left(\frac{f}{f_o} \right)^{1/2} \left(\frac{j_o}{j} \right)^{3/2} \tag{19}$$

NUMERICAL METHOD AND OPTIMIZATION

In this study, the governing equations are solved numerically using a control volume based finite difference formulation, ANSYS FLUENT

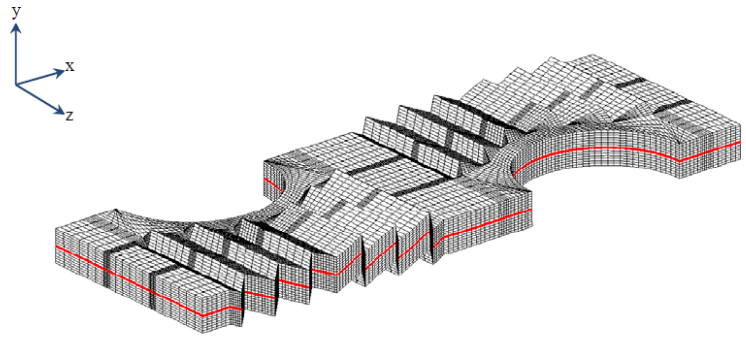

Figure 3. Computational grid system.

(2009). The numerical methodology is briefly described here. Finite difference approximations are employed to discretize the transport equations on non-staggered grid mesh systems. A third-order upwind TVD (total variation diminishing) scheme is used to model the convective terms of governing equations. Second-order central difference schemes are used for the viscous and source terms. A pressure based predictor/multi-corrector solution procedure is employed to enhance velocity–pressure coupling and continuity-satisfied flow filed. A grid system of 288 × 19 × 31 grid points was adopted typically in the computation domain as shown in Figure 3. However, a careful check for the grid-independence of the numerical solutions has been made to ensure the accuracy and validity of the numerical results. For this purpose, three grid systems, 335 × 23 × 37, 288 × 19 × 31 and 241 × 14 × 23, were tested. It was found that for U_{in} = 3.0 m/s, the relative errors in the local pressure and temperature between the solutions of 335 × 23 × 37, 288 × 19 × 31 were less than 3%. The convergence criterion is satisfied when the residuals of all variables are less than 1.0×10^{-7}. Computations were performed on a Pentium 4 3.0G personal computer and typical CPU times were 5000–6000 s.

In the present study, the simplified conjugate-gradient method (Jang and Tsai, 2011) is combined with a finite differential method code (ANSYS FLUENT, 2009) as an optimizer to search the optimum louver angle (θ) and louver pitch (Lp). The objective functions $J(x_1,x_2)$ are defined as the maximum area reduction ratio relative to the palin fin surface $(1\text{-}A/A_o)$.

Above all, the SCGM method evaluates the gradient of the objective function, and then it sets up a new conjugate direction for the updated design variables with the help of a direct numerical sensitivity analysis. The initial guess for the value of each search variable is made, and in the successive steps, the conjugate-gradient coefficients and the search directions are evaluated to estimate the new search variables. The solutions obtained from the finite difference method are then used to calculate the value of the objective function, which is further transmitted back to the optimizer for the purpose of calculating the consecutive searching directions. The procedure for applying this method is described in the following:

(1) Generate an initial guess for two design variables (x_1,x_2) –louver angle (θ) and and louver pitch (Lp).
(2) Adopt the finite difference method to predict the velocity field (U) and temperature fields (T) associated with the latest θ and Lp, and then calculate the objective function $J(x_1,x_2)$.
(3) When the value of $J(x_1,x_2)$ reaches a maximum, the optimization process is terminated. Otherwise, proceed to step 4.
(4) Determine the gradient functions, $(\partial J/\partial x_1)^{(k)}$ and $(\partial J/\partial x_2)^{(k)}$, by applying a small perturbation (Δx_1,Δx_2) to each value of x_1 and x_2, and calculate the corresponding change in objective function (ΔJ). Then, the gradient function with respect to each value of the design variables (x_1,x_2) can be calculated by the direct numerical differentiation as

$$\frac{\partial J_1^{(k)}}{\partial x_1} = \frac{J_1^{(k)} - J^{(k)}}{\Delta x_1} \text{ and } \frac{\partial J_2^{(k)}}{\partial x_2} = \frac{J_2^{(k)} - J^{(k)}}{\Delta x_2} \quad (20)$$

(5) Calculate the conjugate-gradient coefficients $\gamma^{(k)}$, and the search directions, $\xi_1^{(k+1)}$ and $\xi_2^{(k+1)}$, for each search variable. For the first step with k = 1, $\gamma^{(1)} = 0$.

$$\gamma^{(k)} = \frac{\sum_{n=1}^{2}\left(\frac{\partial J_n^{(k)}}{\partial x_n}\right)^2}{\sum_{n=1}^{2}\left(\frac{\partial J_n^{(k-1)}}{\partial x_n}\right)^2} \quad (21)$$

$$\xi_1^{(k)} = \frac{\partial J_1^{(k)}}{\partial x_1} + \gamma^{(k)}\xi_1^{(k-1)} \text{ and } \xi_2^{(k)} = \frac{\partial J_2^{(k)}}{\partial x_2} + \gamma^{(k)}\xi_2^{(k-1)} \quad (22)$$

(6) Assign values to the coefficients of descent direction (β) for all values of the design variables (x_1, x_2). Specifically, those values are chosen by a trial-and-error process. In general, the coefficients of descent direction (β) are within a range of 0.2 ~ 0.01.
(7) Update the design variables with

$$x_1^{(k+1)} = x_1^{(k)} + \beta\xi_1^{(k)} \text{ and } x_2^{(k+1)} = x_2^{(k)} + \beta\xi_2^{(k)} \quad (23)$$

A flowchart of the SCGM optimization process is plotted in Figure 4.

RESULTS AND DISCUSSION

The present study mainly evaluated the influences of louver angle (θ) and louver pitch (Lp) on the local and overall flow and heat transfer characteristics of louver finned and tube heat exchangers. Furthermore, optimization analyses to θ and Lp were utilized in order to search the optimum combination of (θ, Lp) and maximum objective function $(1 - A/A_0)$. The relevant numerical results were achieved in the range of $589 < Re_D < 3533$ ($0.5m/s < U_{in} < 3.0m/s$), $15° < \theta < 40°$, and 2.0 mm < Lp < 3.2 mm. In order to validate the reliability of the numerical

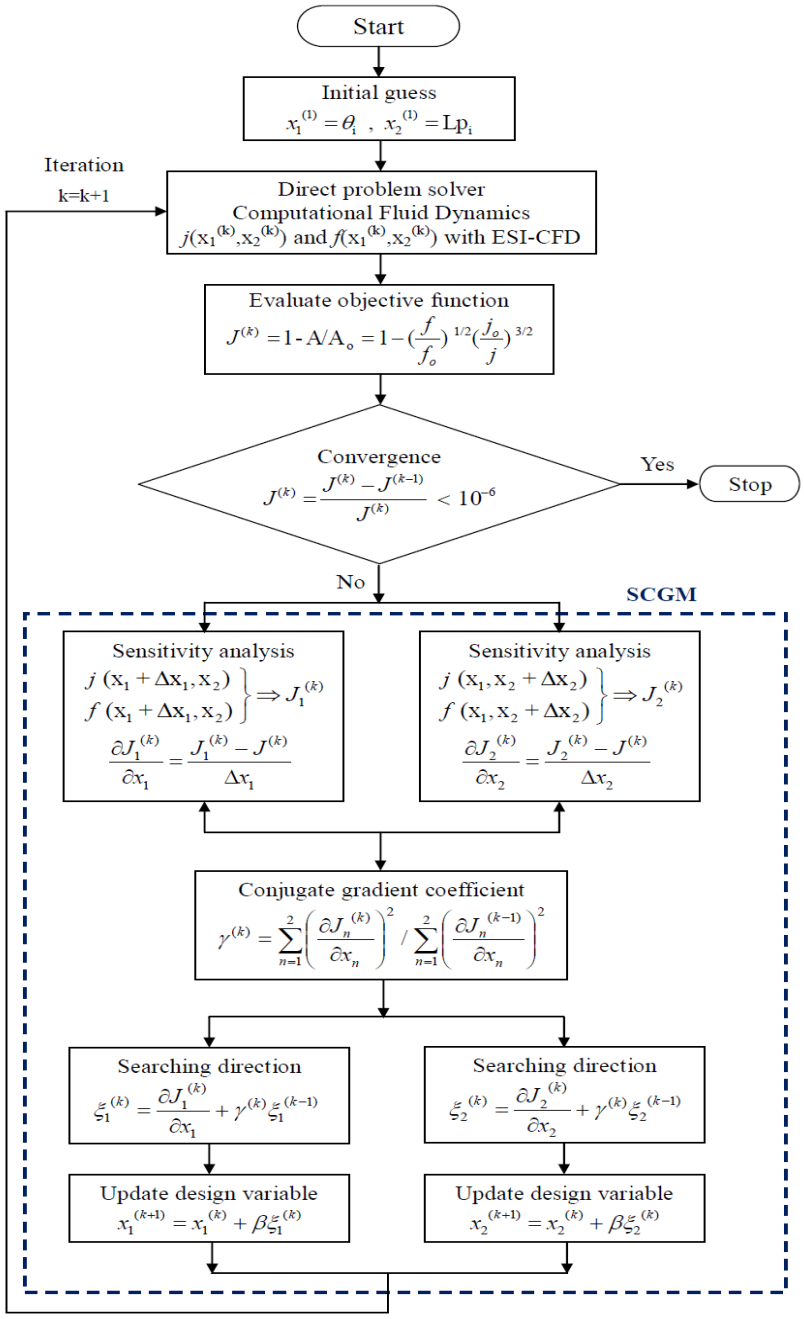

Figure 4. Flowchart for the optimization method.

simulation procedure, numerical simulations were carried out at the same operating conditions as the experimental louver finned-tube heat exchangers with two rows (Wang et al., 1998). Figure 5 shows the comparisons of j and f factors between the simulated results and the experimental results. The present results showed good agreements within a maximum of 10% discrepancy.

The flow and thermal field of a louver finned and tube heat exchanger is very complicated. Figure 6a and b show the streamline velocity and temperature distribution, respectively, for louver finned-tube with U_{in} =3.0 m/s, θ=15° and Lp=2.4 mm. The flow entering a louvered fin array quickly becomes louver directed. Then the flow passing the round cylinder (the first row of tubes) divides into opposite paths of equal velocity and path length over the cylinder surface. Apparently, the streamlines near the tube side wall are very dense and flow velocity accelerates quickly. The reason is that, the geometric shape of the channel near the tube side wall is convergent and divergent. The vortices appear at the downstream behind

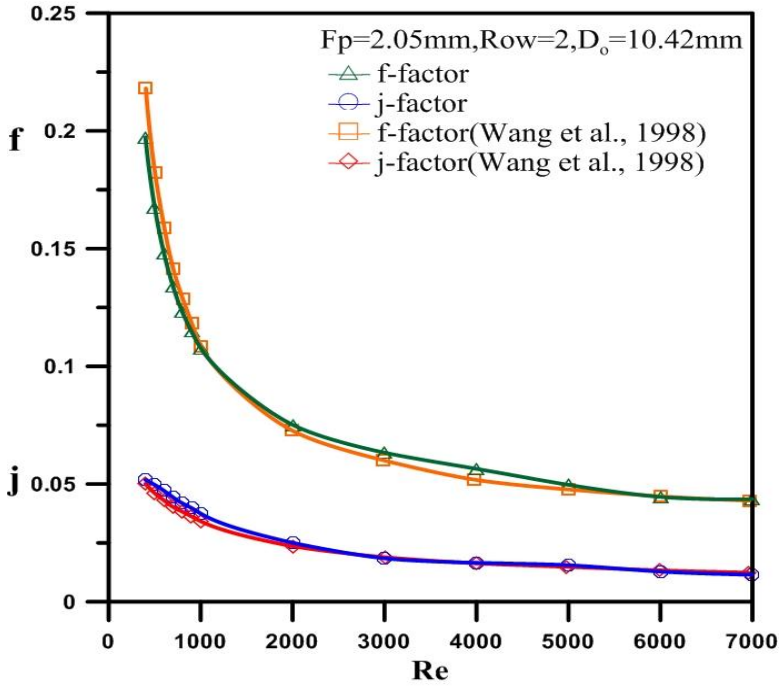

Figure 5. Comparison of the j and f factors for the present study and previous literature.

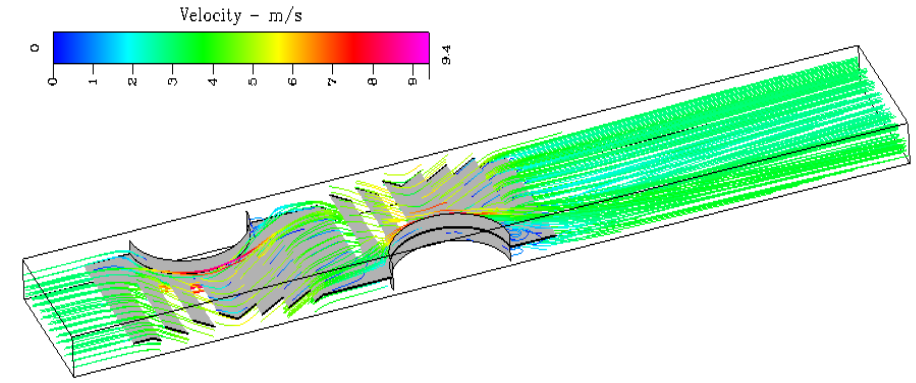

(a)

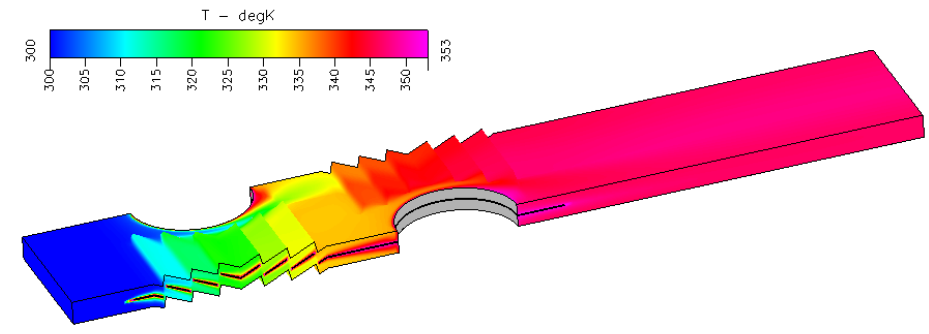

(b)

Figure 6. (a) Streamline velocity and (b) temperature distribution with Re=3533(U_{in}=3.0m/s) for θ = 15° and Lp=2.4 mm.

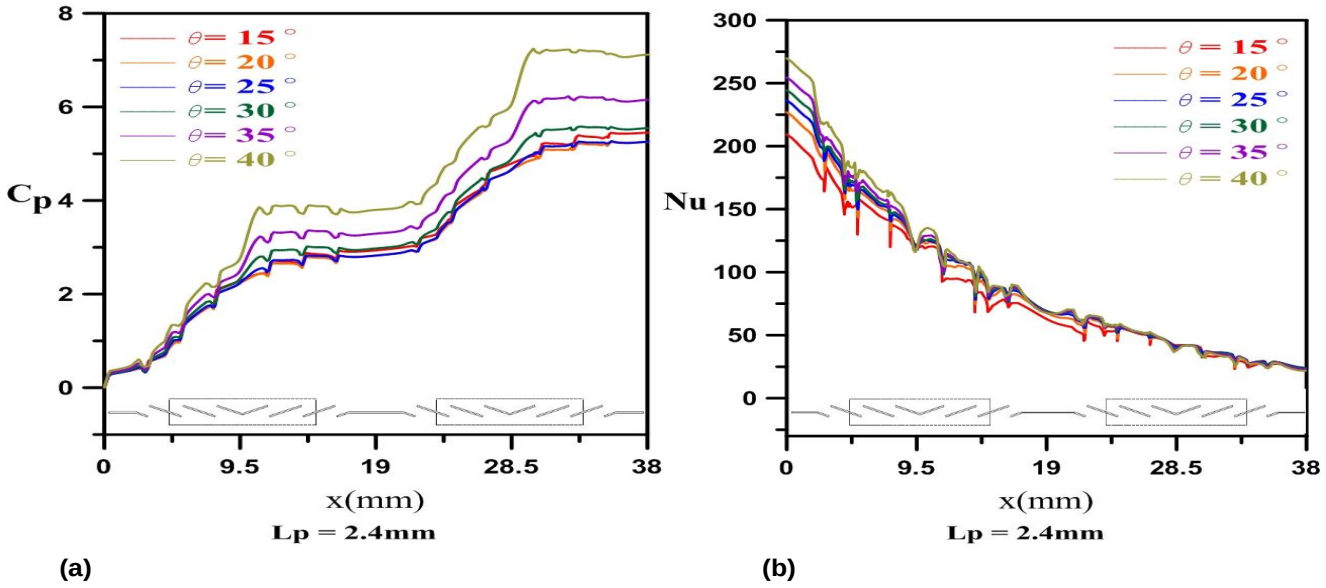

Figure 7. The variation of (a) C_p and (b) Nu along downstream direction for different louver angle with Re=3533(U_{in}=3.0m/s).

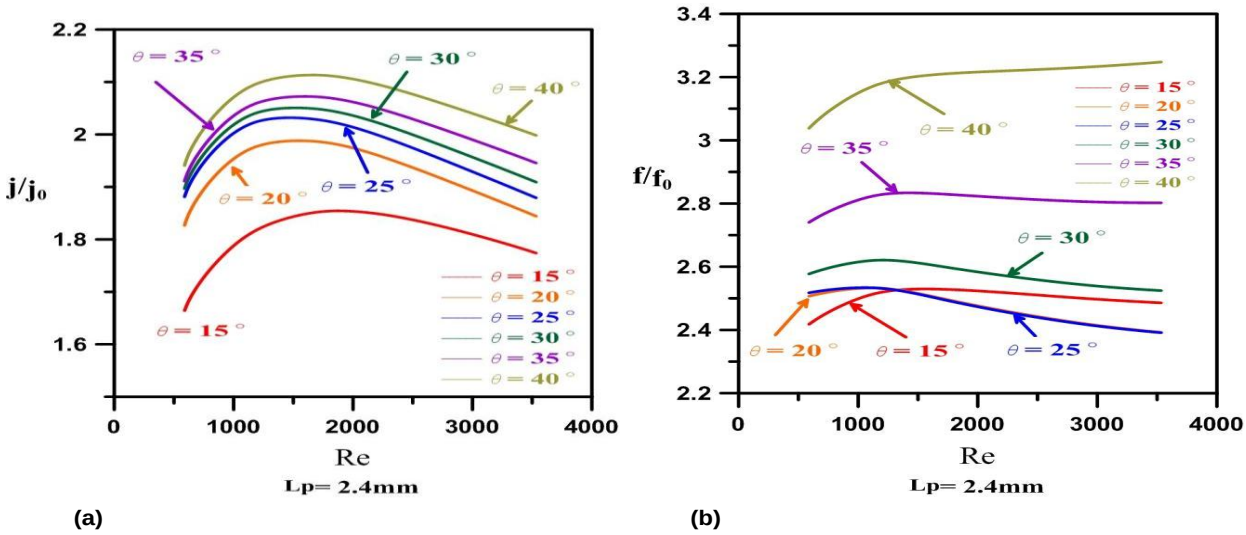

Figure 8. The (a) j/j_o and (b) f/f_o versus Reynolds number for different louver angle (θ) with louver pitch (Lp=2.4 mm).

the tube cylinder. The temperature gradients near the wall are quite large, which indicates a corresponding enhanced heat transfer.

Figure 7a and b present the variations of the local pressure drop coefficient (C_p) and Nusselt number (Nu), respectively, along the downstream direction with inlet frontal velocity (U_{in} = 3.0 m/s) and louver pitch (Lp =2.4 mm) for six different louver angles (θ = 15, 20, 25, 30, 35 and 40°). One can see that the there is a local maximum of Nu at the upstream inlet.

To evaluate how much performance is improved, j/j_o and f/f_o are used to interpret the data, where j/j_o and f/f_0 are the Colburn factor ratio and friction factor ratio between louver and without louver, respectively. Figures 8a and b illustrate the variations of j/j_o and f/f_o, versus Re_D, respectively, for six different louver angles (15, 20, 25, 30, 35 and 40°) with louver pitch (Lp=2.4 mm). The maximum heat transfer improvement interpreted by j/j_o are 1.853, 1.985, 2.026, 2.047, 2.071 and 2.113, and the corresponding friction factor ratio f/f_o are 2.528, 2.494, 2.492, 2.597, 2.829 and 3.211, respectively.

Figure 9a and b illustrate the variations of j/j_o and f/f_o versus Re, respectively, for seven different louver pitch (2.0, 2.2, 2.4, 2.6, 2.8, 3.0, and 3.2 mm) with louver angle

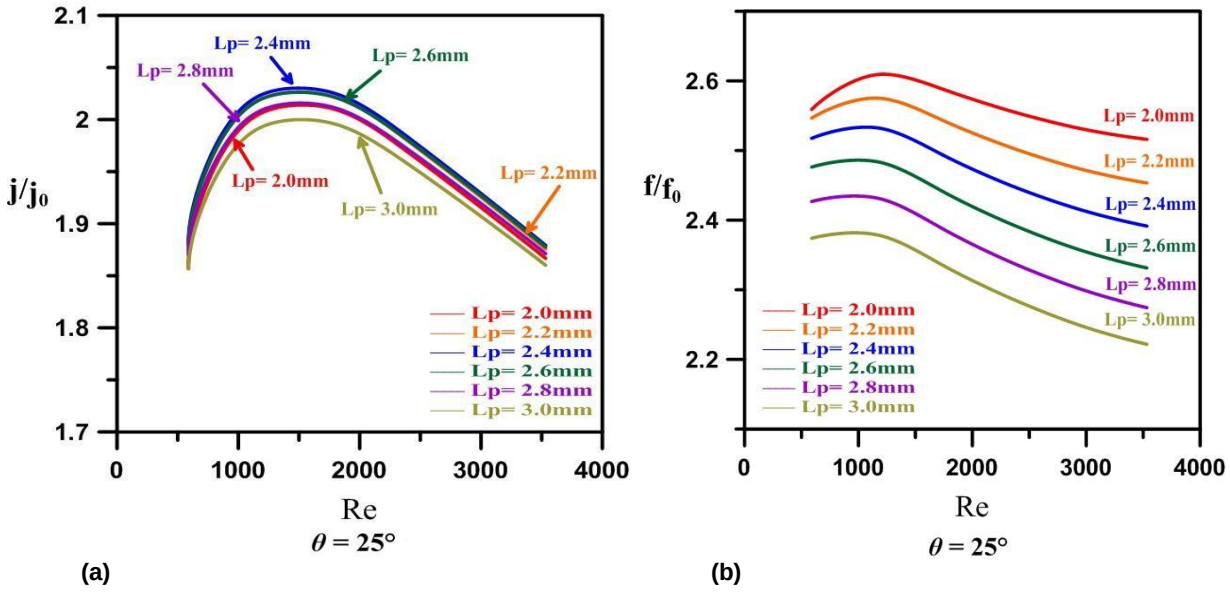

Figure 9. The (a) j/j_o and (b) f/f_o Reynolds number for different louver pitch (Lp) with louver angle (θ=25°).

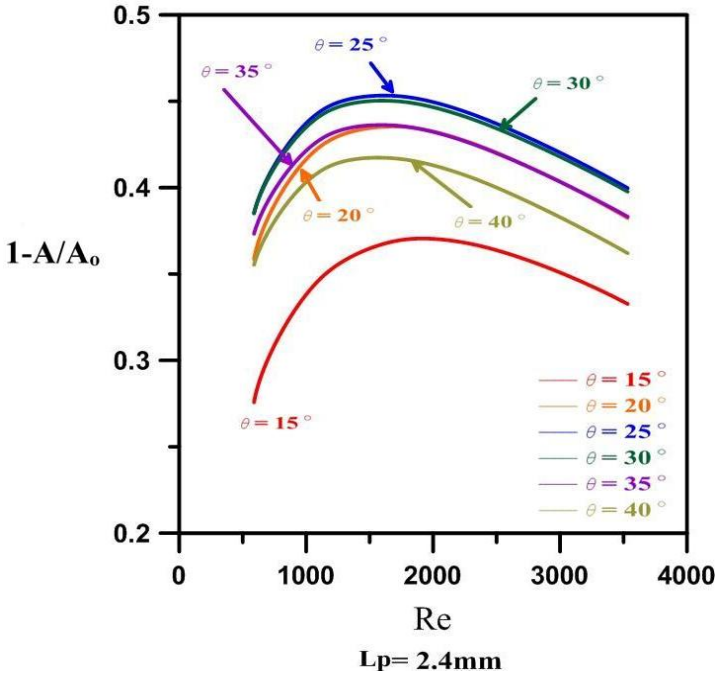

Figure 10. The area reduction versus Reynolds number for different louver angle (θ) with louver pitch (Lp=2.4 mm).

(θ=25°). The maximum heat transfer improvement interpreted by j/j_o are 2.011, 2.023, 2.026, 2.022, 2.012, 1.997 and 1.976, and the corresponding friction factor ratio f/f_o are 2.587, 2.541, 2.492, 2.439, 2.385, 2.333 and 2.286, respectively. The present results indicated that the variable louver angle and pitch patterns applied in heat exchangers could effectively enhance the heat transfer performance.

The possible area reduction $1-A/A_o$ (where A and A_o denote the surface areas for variable louver θ ranging from 15 to 40° and conventional plain fins, respectively) with Lp = 2.4 mm is presented in Figure 10. One can see

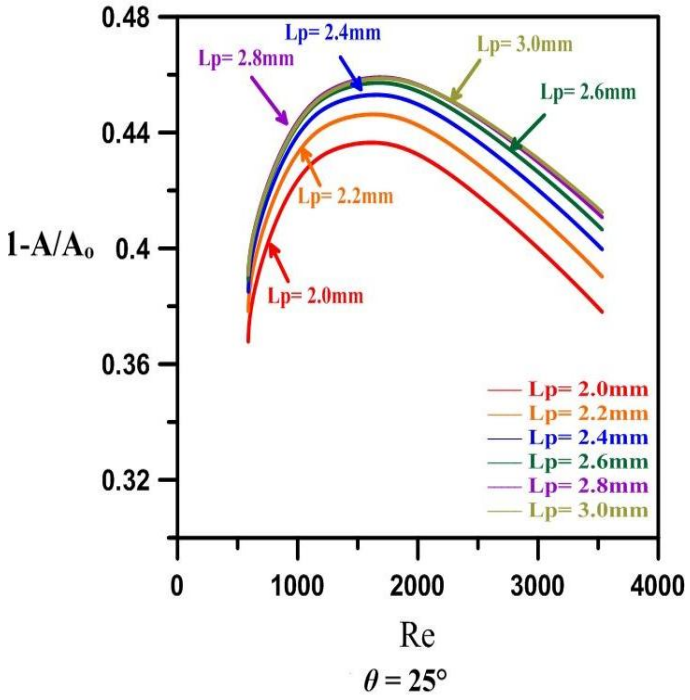

Figure 11. The area reduction versus Reynolds number for different louver pitch (Lp) with louver angle (θ=25°).

that the greatest area reduction ratio is as much as 37.0, 43.5, 45.3, 45.0, 43.5 and 41.6% with specific values of Re_D = 589, 1178, 1766, 2355, 2944 and 3533, respectively, it gives the greatest area reduction at Re = 1766 and θ =25°. Figure 11 presents the area reduction ratio for Lp ranging from 2.0 to 3.2 mm with θ = 25°, the greatest area reduction ratio is as much as 43.6, 44.6, 45.3, 45.7, 45.9, 45.9 and 45.6% with specific values of Re = 589, 1178, 1766, 2355, 2944 and 3533, respectively, it gives the greatest area reduction at Re = 1766 and Lp=3.0 mm.

Figure 12 displays the iteration process used to search the optimum louver angle (θ) and louver pitch (Lp) combination for the maximization of objective function (that is, area reduction ratio, $1-A/A_o$) at Re_D = 1766 (U_{in} = 1.5 m/s). The constant area reduction ratio contours are plotted as a function of θ and Lp, where the dark red area represents the maximum area reduction ratio. It is seen that, with the initial values (θi = 15° ,Lpi = 3.0 mm) and (θi = 40°, Lpi = 3.0 mm), by using the simple conjugated gradient method (SCGM), the optimal θ and Lp combination is obtained (θ = 24.09°, Lp = 2.91 mm) for around 19 and 18 iterations, respectively. The area reduction ratio is 45.9%. Thus, the current optimization method provides a tremendous savings in regard to computational time for the present physcial model. The searched optimum combination of θ and Lp with specific values of Re_D = 589, 1178, 1766, 2355, 2944 and 3533 (U_{in}=0.5 to 3.0 m/s) are tabulated in Table 1. It is seen that, an area reduction ratio of 39 to 46% is achieved across the range of Re_D.

Conclusion

Three dimenional turbulent fluid flow and heat transfer in two row fin-and-tube heat exchanger with and without louver fins are studied numerically. The optimization of the louvered angle (θ) and louvered pitch (Lp) is executed by using a simplified conjugate-gradient method. A searched procedure for the optimum louver angle (θ) and louver pitch (Lp), ranging from 15°< θ < 40° and 2.0 mm < Lp < 3.2 mm, respectively, is executed. The searched optimum objective function associated with an optimal combination of θ and Lp for different Re_D are obtained for less than 30 iterations. This demonstrates that the current optimization method provides a tremendous savings in regard to computational time for the present physcial model. In addition, the results showed that the maximum area reduction ratios may reach 39~46% combined with the optimal design of (θ, Lp) at U_{in}= 0.5~3.0 m/s.

ACKNOWLEDGEMENT

Financial support for this work was provided by the National Science Council of Taiwan, under contract NSC NSC 101-2221-E-006 -109 -MY2.

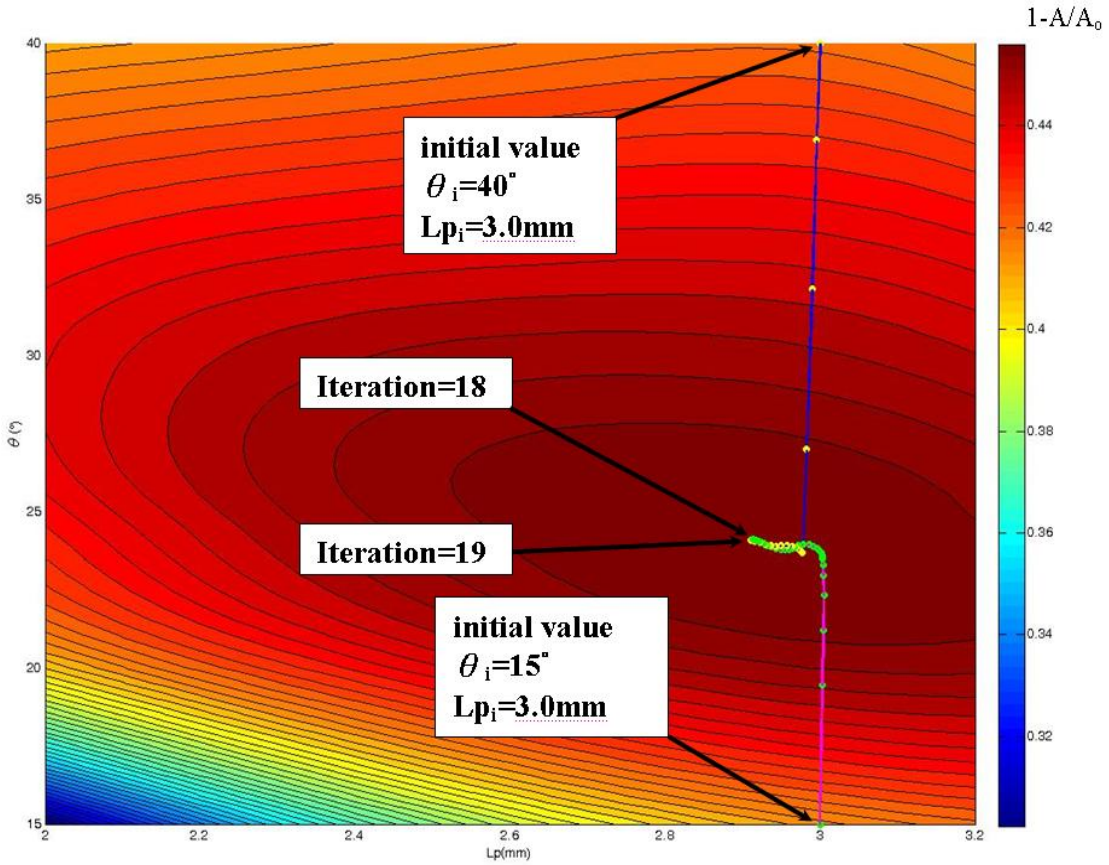

Figure 12. Iteration process to search the optimum combination of θ and Lp (U_{in}=1.5m/s).

Table 1. The searched optimum combination of θ and Lp for different Re_D.

Re	U_{in}(m/s)	Initial value		θ	Lp(mm)	j/j_o	f/f_o	1-A/A$_o$ (%)	Iteration numbers
		θ_i	Lp$_i$						
589	0.5	15.0	3.0	25.11	2.93	1.862	2.393	39.1	29
1178	1.0	15.0	3.0	24.23	2.88	2.003	2.411	45.2	25
1766	1.5	15.0	3.0	24.09	2.91	2.004	2.353	45.9	19
2355	2.0	15.0	3.0	24.10	2.97	1.963	2.291	45.0	18
2944	2.5	15.0	3.0	24.47	2.98	1.912	2.251	43.3	13
3533	3.0	15.0	3.0	24.80	2.99	1.859	2.220	41.2	14

Nomenclature: A, total surface area (m^2); **C,** fluid heat capacity (J /kg°C); **Cp,** pressure drop coefficient; D_o, outside diameter of tube (m); ***f,*** friction factor; **h,** heat transfer coefficient (W/m^2°C); **j,** Colburn factor; **k,** thermal conductivity (W/m°C); **Lp,** louver pitch (m); **Nu,** local Nusselt number, hD_o/k; $\overline{Nu}$ **,** average Nusselt number; **P,** pressure (Pa); **Pr,** Prandtl number, v/α; **q,** heat flux (W/m^2); $\mathbf{Re_D}$**,** Reynolds numbers, $U_{max}D_o/v$; **T,** temperature (°C); $\mathbf{T_w}$**,** wall temperature (°C); $\mathbf{T_{in}}$**,** inlet temperature (°C); $\mathbf{T_b}$**,** bulk mean temperature (°C); $\mathbf{U_{in}}$**,** frontal velocity (m/s); $\mathbf{U_{max}}$**,** air velocity at minimum flow area (m/s); **x,y,z,** coordinates; **α,** thermal diffusivity (m^2/s); **θ,** louver angle (degree); **v,** kinematic viscosity (m^2/s); **ρ,** density of fluid (kg/m^3); **μ,** dynamic viscosity (kg/ms).

REFERENCES

Achaichia A, Cowell TA (1988). Heat transfer and pressure drop characteristics of flat tube and louvered plate fin surfaces, Experimental Thermal Fluid Sci. 1:147-157.

ANSYS FLUENT (2009). A Release 12.0, Documentation for ANSYS Workbench. ANSYS Ltd.

Chen YS, Kim SW (1987). Computation of Turbulent Flows Using an Extended K - ε turbulence Closure Model NASA CR-179204.

Davenport CJ (1983). Correlations for heat transfer and flow friction characteristics of louvred fin, AIChE Symposium Series. 19-27.
Hiramatsu M, Ishimaru T, Matsuzaki K (1990). Research on fins for air conditioning heat exchangers. JSME Int. J. Ser. II, 33:749-756.
Hsieh CT, Jang JY (2006). 3-D thermal-hydraulic analysis for louver fin heat exchangers with variable louver angle. Appl. Thermal Eng. 26:1629–1639.
Hsieh CT, Jang JY (2012). Parametric study and optimization of louver finned-tube heat exchangers by Taguchi method, Appl.Thermal Eng. 42:101-110.
Ikuta S, Sasaki Y, Tanaka K, Takagi M, Himeno R (1990). Numerical analysis of heat transfer around louver assemblies. Int. Congress & Exposition Tech., Detroit, Michigan, USA.
Jang JY, Shieh KP, Ay H (2001). 3-D thermal-hydraulic analysis in convex louver finned -tube heat exchangers, ASHRAE Annual Meeting, Cincinnati, OH, USA, June 22-27, pp. 501-509.
Jang JY, Tsai YC (2011). Optimum Louver Angle Design for a Louvered Fin Heat Exchanger, Int. J. Phys. Sci. 6:6422-6438.
Kays WM, London AL (1950). Heat transfer and flow friction characteristics of some compact heat exchanger surfaces-part I: test system and procedure, Trans. ASME 72:1075-1085.
Liakopoulos A (1984). Explicit representation of the complete velocity profile in a turbulent boundary layer, AIAA J. 22:844-846.
Sahnoun A, Webb RL (1992). Prediction of heat transfer and friction for louver fin geometry, ASME Journal of Heat Transfer 114:893-900.
Suga K, Aoki H, Shinagawa T (1990). Numerical analysis on two dimensional flow and heat transfer of louvered fins using overlaid grids. JSME Int. J. Ser. II, 33:122-127.
Suga K, Aoki H (1991). Numerical study on heat transfer and pressure drop in multilouvered fins. In Proceed. of ASME/JSME Thermal Eng. Joint Conf. 4:361-368.
Sunden B, Svantesson J (1992). Correlation of j- and f- Factors for multilouvered heat transfer surfaces. In proceedings of the 3rd UK National Heat Transfer Conf. 805-811.
Wang CC, Chi KY, Chang YJ (1998). An experimental study of heat transfer and friction characteristics of typical louver finned-tube heat exchangers, Int. J. Heat Mass Transfer. 41:817-822.
Wang TS, Chen YS (1993). Unified Navier-Stokes flowfield and performance analysis of liquid rocket engines, AIAA J. 9:678-685.
Webb RL (1994). Principles of Enhanced Heat Transfer, New York, John Wiley & Sons.